Spiral wave drift induced by high-frequency forcing. Parallel simulation in the Luo–Rudy anisotropic model of cardiac tissue[*]

Timofei Epanchintsev[1,2], Sergei Pravdin[1,2], and Alexander Panfilov[3]

[1] Krasovskii Institute of Mathematics and Mechanics, Ekaterinburg, Russia
[2] Ural Federal University, Ekaterinburg, Russia
[3] Ghent University, Ghent, Belgium

Abstract. Non-linear waves occur in various physical, chemical and biological media. One of the most important examples is electrical excitation waves in the myocardium, which initiate contraction of the heart. Abnormal wave propagation in the heart, such as the formation of spiral waves, causes dangerous arrhythmias, and thus methods of elimination of such waves are of great interest. One of the most promising methods is so-called low-voltage cardioversion and defibrillation, which is believed to be achieved by inducing the drift and disappearance of spiral waves using external high-frequency electrical stimulation of the heart. In this paper, we perform a computational analysis of the interaction of spiral waves and trains of high-frequency plane waves in 2D models of cardiac tissue. We investigate the effectiveness and safety of the treatment. We also identify the dependency of drift velocity on the period of plane waves. The simulations were carried out using a parallel computing system with OpenMP technology.

Keywords: anisotropy, spiral wave, overdrive pacing, heart model, low-voltage cardioversion, wave drift

1 Introduction

Mechanical contraction of the heart is caused by electrical excitation of myocardial cells. The electrical waves propagate through the entire myocardium and initiate coordinated cardiac contraction. In normal conditions, such waves originate at the natural pacemaker of the heart, the sinus node, located in the right atrium, and propagate through all cardiac tissue. However, in some cases abnormal cardiac excitation sources can occur. One source is rotating spiral waves, which can appear in the myocardium as a result of special conditions, such as the formation of a regional block for the propagating excitation wave. A spiral wave is a vortex that rotates at abnormally high frequency. It causes dangerous cardiac arrhythmias, such as paroxysmal tachycardia or fibrillation. In some cases, spiral waves can disappear spontaneously, and arrhythmia stops by itself.

However, if this does not occur, an urgent medical intervention is necessary. In this regard, it is very important to develop effective ways to control the dynamics and position of the spiral waves in the heart, as it will result in the development of better ways of managing these diseases.

There are three classical methods of treatment of such rhythm disturbances: anti-arrhythmic drugs, surgery and electrical therapy. Electrotherapy is called 'defibrillation' or 'cardioversion'. There are three kinds of electrotherapy devices: external (electrodes are applied on the skin of the chest or the back of the patient), surgical (the paddles placed directly on the heart; it is mostly used in the operating room) and implantable (small devices under the skin whose electrodes are inserted into myocardium). These methods have serious disadvantages, as defibrillation and cardioversion require huge voltages (up to several kilovolts), which can damage the heart. Therefore, there is a long-standing interest in development of low-voltage cardioversion-defibrillation (LVCD). The idea of LVCD is to overdrive spiral waves using trains of plane waves induced by external stimulation from one or multiple electrodes. This method uses low voltage ($\approx$10V) and does not damage the heart and is much more tolerable by the patients. The LVCD methods were proposed on the basis of theoretical studies of waves in active media. Previously, the theory of LVCD has been developed for the case of isotropic 2D medium [4, 6]. The LVCD method also has been tested in clinical settings [24, 21].

A spiral wave can rotate around an unexcitable obstacle, for example, around a scar after myocardial infarction. There are theoretical results in 2D and 1D models of the anchored spirals [20]. Stimulation from a point electrode is one method of LVCD. Another method is based on the effect of application of an external electric field to the entire myocardium [2, 7, 8]. In such case, spiral waves unpin from unexcitable obstacles and start moving toward the boundary. It is known that the stimulation is more effective if the electrode is placed near the spiral wave core. This phenomenon was numerically studied in [27, 6].

Spiral waves can appear not only in the myocardium but also in chemical media. For example, the stabilization and destabilization of spiral waves in the Belousov–Zhabotinsky reaction has been studied [9]. Control of spiral waves in confined media was investigated in [28].

However, the aforementioned works considered control processes with simplified models of excitable media and neglected some specific features of the myocardium. In particular, there are no studies about the effects of anisotropy, no research in realistic 3D heart models and no studies using biophysical models of cardiac cells, which should include a description of ionic currents and intercellular interaction. Moreover, electromechanical feedback was not studied, though it strongly affects the spontaneous drift of spiral waves. These limitations can explain the discrepancy between the theory and experimental studies [25, 11].

Previously, we studied the induced drift of spiral waves in the isotropic myocardium using simple phenomenological Aliev–Panfilov models [18]. The next step was to check how a simple anisotropic structure based on parallel fibres influences the drift [3].

The speed of electrical excitation is 2–4 times larger along than across the fibres, so the myocardium is highly anisotropic. Moreover, myocardial fibres in the heart are not parallel and have different patterns. The present work is devoted to studying LVCD in anisotropic myocardium models with curved fibres. We used a biophysical ionic Luo–Rudy cell model [12]. After measuring the time of the beginning and end of the spiral drift and determining the type of overall reaction of the spiral on the stimulation, we compare our findings with the results for the isotropic and parallel fibres-based anisotropic cases [18, 3].

The implemented program was parallelised using OpenMP technology. Since the heart simulation task is computationally intensive, we used a high-performance computing system for simulations.

2   Materials and Methods

2.1   Electrophysiological Model

We used a well-known biophysical model of the cardiomyocyte 'Luo–Rudy I' LR-I [12]. Propagation of wave excitation in the tissue was modelled using monodomain reaction–diffusion equations:

$$\frac{\partial u}{\partial t} = \mathrm{div}(D \,\mathrm{grad}\, u) - \frac{I_{\mathrm{ion}} + I_{\mathrm{stim}}(\boldsymbol{r}, t)}{C_m}, \tag{1}$$

$$I_{\mathrm{ion}} = I_K + I_{Kp} + I_{K1} + I_{Na} + I_b + I_{si}, \tag{2}$$

where $u = u(\boldsymbol{r}, t)$ is the transmembrane potential at the point $\boldsymbol{r} = (x, y)$ at the time t, I_{ion} is the sum of ionic currents, C_m is membrane capacitance and $I_{\mathrm{stim}}(\boldsymbol{r}, t)$ is the external stimulation current.

The original LR-I model was modified as proposed in [22]. We used $g_K = 0.705$ instead of $g_K = 0.282$ and $g_{si} = 0.045$ instead of $g_{si} = 0.09$. This made it easier to make a spiral wave in the 2D domain in comparison with the original parameter set, which provided a spiral wave with a very irregular trajectory.

To model anisotropic conduction along cardiac myofibres, we used a uniaxially anisotropic diffusion tensor D with Cartesian components $D^{ij} = D_a \delta_{ij} + (D_f - D_a)\boldsymbol{w}^i \boldsymbol{w}^j$, $i, j = 1, 2$, where δ_{ij} is the Kronecker symbol and $\boldsymbol{w} = \boldsymbol{w}(\phi) = (\cos\phi, \sin\phi)$ is the unit vector of the myofibre direction. Consequently, the diffusion coefficient is maximal and equal to D_f along $\boldsymbol{w}$, and it is minimal and equal to D_a in the transverse direction. For the anisotropy, $D_f > D_a$, and for the isotropy, $D_f = D_a$. Fibres were arcs of circles with the centre at $(0, 0)$, so the fibre direction angle was $\phi(x, y) = \mathrm{atan2}(y, x) + \pi/2$.

At the medium boundaries, no-flux conditions $\boldsymbol{n} \cdot D \,\mathrm{grad}\, u = 0$ were imposed with the local normal vector $\boldsymbol{n}$.

The stimulation current $I_{st} = 90\ \mu\mathrm{A/cm^2}$ was applied on region Ω_{stim} with period T_{stim} by impulses with a duration $t_{\mathrm{stim}} = 1.5$ ms starting from the moment $\tau_0 = 600$ ms when the spiral captured the entire computational space:

$$I_{\mathrm{stim}}(x, y, t) = \begin{cases} I_{st}, & \text{if } (x, y) \in \Omega_{\mathrm{stim}},\ t \geqslant \tau_0,\ \left\{\frac{t - \tau_0}{T_{\mathrm{stim}}}\right\} \leqslant \frac{t_{\mathrm{stim}}}{T_{\mathrm{stim}}}; \\ 0, & \text{otherwise.} \end{cases}$$

We found the minimal value $I_{min} = 20$ $\mu A/cm^2$ of the current which caused action potential. Then, we set $I_{st} := 4.5I_{min}$. The stimulation was started when the spiral wave 'controlled' the entire computational domain.

It is known that any spiral wave has a tip where the wavefront and waveback meet. The spiral tip rotates around an area called the 'core'. A spiral wave is considered drifting if its core moves. Studying the dynamics of spiral waves is usually simplified by exploring the trajectory of the tip. To find it, we specified a certain level $u^* = -40$ mV of the transmembrane potential, then the tip position $\boldsymbol{r}_{tip}$ was approximated by the following equations [5]:

$$u(\boldsymbol{r}_{tip}, t) = u^*, \qquad u(\boldsymbol{r}_{tip}, t + \Delta t) = u^*,$$

where $\Delta t = 2$ ms. The trajectory of the tip motion helps to determine the average drift velocity of the spiral wave and the type of its dynamics.

2.2   Computational Experiments

As electrical signals in the heart propagate faster along myofibres than across them, our model 2D square was anisotropic. The diffusion coefficients were $D_f = 0.16$ mm^2/ms and $D_a = 0.04$ mm^2/ms. The reaction–diffusion system was integrated using the finite difference and the explicit Euler methods with time step $dt = 0.005$ ms, space step $dr = 0.25$ mm and a mesh size 100×100 mm.

The S1S2 protocol [15] was used to make spiral waves. First, the S1 stimulus induces a plane wave, which propagates from one side of a square to another. Then, S2 is given so that it crosses the back-front of the first plane wave. A spiral wave appears near the intersection. Stimulus S1 was applied to the left part of the square $x < 50$ mm. Stimulus S2 was applied to the bottom half of the square $y < 50$ mm at the time 158 ms.

The LR-I model is one of the most widely used models in large-scale computational cardiology and reproduces cardiomyocyte excitation in various conditions.

In Table 1, we specify action potential durations APD-90, speeds of 1D waves, temporal periods of spiral waves and filament tensions for LR and ten Tusscher–Panfilov (TP06) [23] biophysical models of the myocardium. The data on the TP06 model are taken from [18]. The APD-90 is the duration of time of one action potential when the cell potential $u(t)$ relative to its resting state value u_{min} is higher than 10% of its range $u_{max} - u_{min}$:

$$u(t) - u_{min} > 0.1(u_{max} - u_{min}).$$

We see that the APD-90 and T_{sw} values in LR-I are smaller than in TP06, but the spatial and 3D stability characteristics, V_1 and tension, are the same.

An important characteristic of a spiral wave is its temporal period T_{sw}. It is known that the period of a non-drifting wave is equal to the period of oscillations of the model phase variables outside the core of the spiral. We calculated the period of spiral waves as the time between the maxima of the transmembrane potential averaged by ten periods, at a point outside the stimulation region and outside the core of the wave. We set the period of external stimulation relatively

Table 1. Parameters and characteristics of the isotropic myocardial models

Model	APD-90, ms	1D wave speed V_1, mm/ms	Spiral wave period T_{sw}, ms	Tension, mm^2/ms
LR-I	148	0.74	61	0.55
TP06	292	0.68	249	0.6

to T_{sw}: $T_{stim} = p \cdot T_{sw}$, where $0.85 \leq p \leq 1.04$. Also, we measured the spiral wave period in two anisotropic models, one with the straight fibres and one with the curved fibres, and obtained the same values as in the isotropic model.

An example of a spiral wave for an arc-like fibre pattern is shown in Fig. 1. Fibres are highlighted by black lines. We see that the spiral wave front does not look like an Archimedean spiral but follows the fibre pattern to an extent. A fragment of the spiral wave tip trajectory is presented in Fig. 2. We see no distinct core shape, but the spiral seems to drift slowly enough to induce its drift with a greater speed.
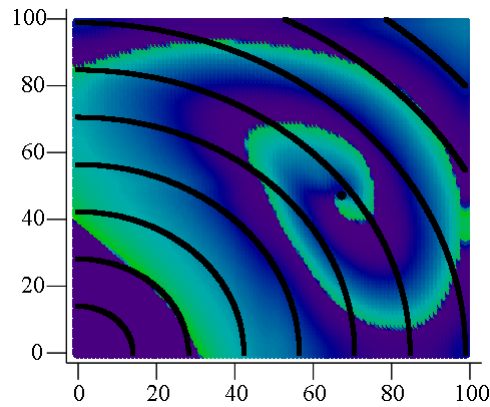

Fig. 1. Spiral wave and fibre directions (black curves) before the overdrive pacing began. The black dot shows the position of the tip. X- and Y-axes are in mm.

We wrote our program in the C language (C99 version) and compiled it using the Intel compiler icc. The most overloaded code sections were determined and accelerated using OpenMP, which decreased the simulation time significantly. We used a computational node whose configuration is presented in Table 2. The program has a nearly linear scalability (tested by simulation of 5000 ms and one stimulation electrode at the left bottom square corner). Table 3 shows simulation times with different numbers of cores. We achieved ≈ 21x time speedup on 32 cores. Such scalability is explained by the computational intensiveness of the task and by the independence of each subtask delegated to the computing nodes. The acceleration ratio is similar to the ratio for the Aliev–Panfilov (AP) model
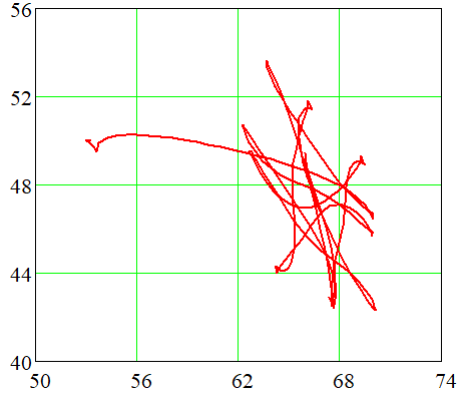
Fig. 2. Spiral wave tip trajectory in the anisotropic myocardial model with curved fibres. 0.25 seconds were simulated. X- and Y-axes are in mm.

because we used the same size of mesh (400×400 nodes), thus, each computing node had a subtask of the same size. However, the overall calculation time in the LR-I model is significantly greater than that in AP model since it is more sophisticated.

All simulations were carried out on a single node of the *Uran* supercomputer of the Krasovskii Institute of Mathematics and Mechanics.

Table 2. Configuration of the computational node

CPU	6 x Intel(R) Xeon(R) CPU E5-2697 v4 @ 2.30GHz
RAM	252 GB
Operating System	CentOS 7.3

Table 3. The simulation time and achieved speedup using OpenMP

Number of cores	1	2	4	8	16	32
Simulation time, s	42215	21716	10992	6155	3542	1973
Acceleration ratio	1	1.9	3.8	6.9	11.9	21.4

3   Results

The anisotropic structure with curved fibres can cause spontaneous drift of spiral waves. We simulated spiral wave dynamics for 60 seconds without the external stimulation and plotted a spontaneous drift trajectory. The results are shown in Fig. 3. The spiral wave was drifting along the fibres until it reached the boundary.

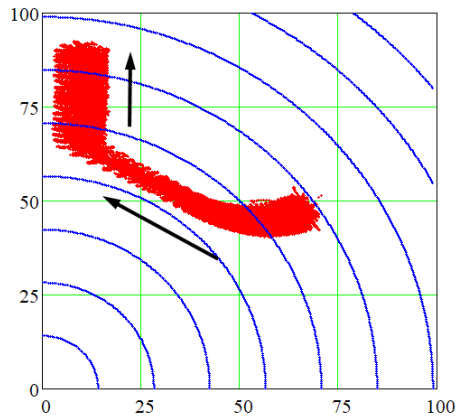In our experiments, we used two electrode locations:

Fig. 3. Spontaneous drift of a spiral wave. No external stimulation. Fibres are shown as blue curves. Arrows show drift directions. X- and Y-axes are in mm.

1. One point electrode at the left bottom square corner (Fig. 4, left).
2. One line electrode located at the left edge of the square (Fig. 4, right).

   We use the following notations for response types of spiral waves.

A: spiral drifted from the electrode and disappeared at the boundary;
B: a drift to the boundary of the square, then along the boundary;
D: no effect;
E: a spiral wave breakup;
An: n new spirals arose and vanished whereas the main spiral response was A.

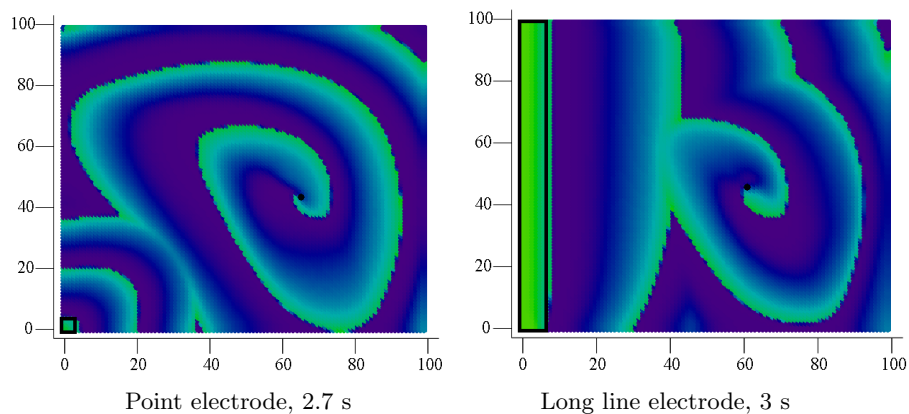Point electrode, 2.7 s   Long line electrode, 3 s

Fig. 4. Interaction of spiral waves with the trains of plane waves. Electrodes are shown in black rectangles. X- and Y-axes are in mm.

In our previous work [18], we also observed a drift to the boundary and stop (type C). However, we did not observe this type of dynamics in the current work. Fig. 5 illustrates the wave types A, An and E. The fourth picture shows spontaneous drift toward the left boundary and the drift induced by the point electrode.
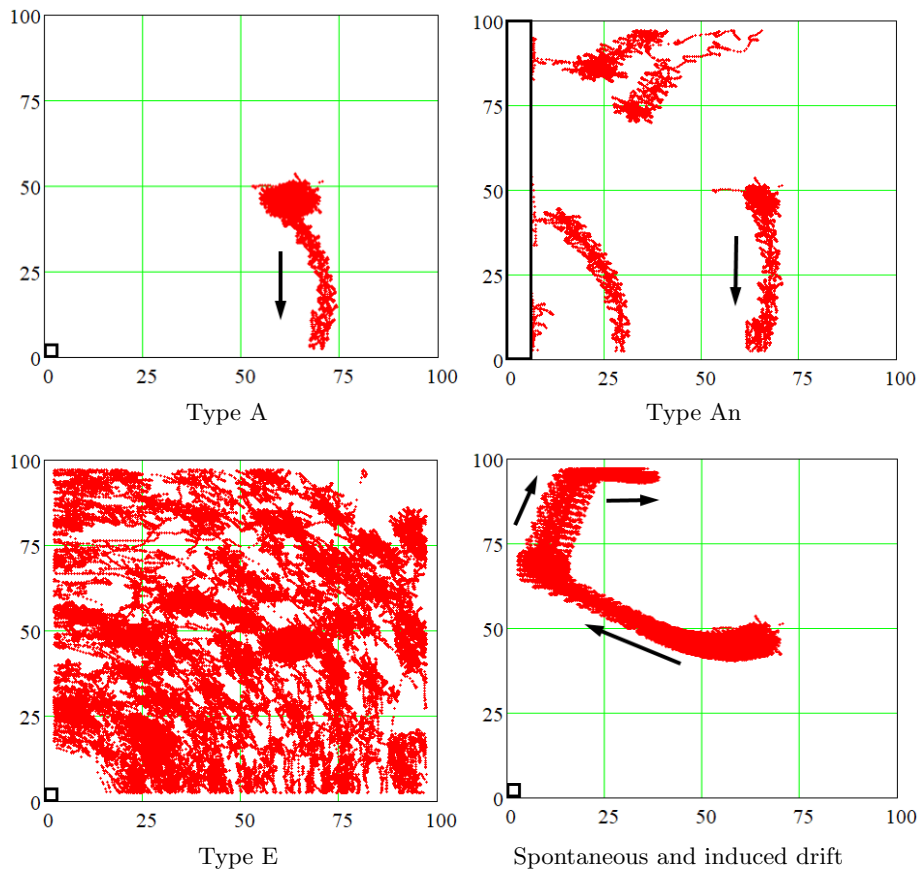

Fig. 5. Spiral wave response types. Red points show tip trajectories. Rectangles display positions of the electrodes. The electrodes were point (type A, type E, and spontaneous and induced drift) and long line (type An). Relative stimulation periods are: 0.96 (type A), 0.93 (type An), 0.85 (type E; multiple red regions represent cores of multiple spiral waves which occur as a result of the spontaneous breakup) and 1.01 (spontaneous and induced drift). Arrows show drift directions. X- and Y-axes are in mm.

Results of the computational experiments are shown in Tables 4–6. For both electrode configurations, the relative period 0.85 caused spiral wave breakup. When the periods exceeded 1.04, no effect was observed for the point electrode, and breakup occured for the linear electrode.

Table 4. Response types of spiral wave

Relative stimulation period	Electrode configuration	
	Point electrode	Long line electrode
0.85	E	E
0.88	E	An
0.905	A7	A2
0.93	A	A3
0.96	A	A1
0.985	A or B?	A1
1.01	B	B
1.04	D	E

Table 5. Time when the spiral began and ended its drift, seconds

Relative stimulation period	Electrode configuration			
	Point electrode		Long line electrode	
	start	end	start	end
0.85	—	—	—	—
0.88	—	—	2.1	3.2
0.905	4.8	5.7	2.6	4.2
0.93	6.4	8.4	3.2	5.6
0.96	10	13.3	4.9	7.5
0.985	27	> 60	10.4	17.8
1.01	40	46	40.7	45.9
1.04	—	—	—	—

Table 6. Spiral wave's absolute and relative drift velocity components for the case of one line electrode

Relative stimulation period	Total V_x, mm/ms	Net V_x, mm/ms	Net V_x^{rel}	Total V_y, mm/ms	Net V_y, mm/ms	Net V_y^{rel}
0.85	—	—	—	—	—	—
0.88	0.007	0.0087	0.013	−0.045	−0.0455	−0.067
0.905	0.001	0.0027	0.004	−0.025	−0.0255	−0.038
0.93	−0.001	0.0007	0.001	−0.017	−0.0175	−0.026
0.96	−0.001	0.0007	0.001	−0.016	−0.0165	−0.024
0.985	−0.0016	0.0001	0.0001	−0.006	−0.0065	−0.010
1.01	0.0017	0.0034	0.005	0.0047	0.0042	0.006
1.04	—	—	—	—	—	—

The segment of effective relative periods for the point electrode was 0.905–0.96. However, in case of $T_{\mathrm{stim}} = 0.905 \cdot T_{\mathrm{sw}}$, seven spiral waves appeared near the NW and SE corners (the electrode was at the SW corner), although they disappeared before the end of the simulation. For the relative period $T_{\mathrm{stim}} = 1.04 \cdot T_{\mathrm{sw}}$ and the point electrode, there was a spontaneous spiral wave drift toward the boundary, but no induced drift was observed. Hence, this case was defined as D type. Stimulation with $T_{\mathrm{stim}} = 0.985 \cdot T_{\mathrm{sw}}$ induced a very slow drift, and the spiral still did not reach the boundary after 60 s, so we marked this case as 'A or B?'.

In the case of the long line electrode, we did not achieve pure A type. All spiral wave drifts were followed by additional spiral waves, which also disappeared. The segment of effective relative periods was 0.88–0.985. Type An for $T_{\mathrm{stim}} = 0.88 \cdot T_{\mathrm{sw}}$ means that multiple spiral waves arose, which shows a high chance of breakup. In A cases, new spiral waves emerged near the long line electrode and far from it.

We checked that the effective stimulation with the minimal relative period, which was 0.88, worked without the Wenckebach/Mobitz pattern [26]. A plot of transmembrane potential is shown in Fig. 6. We considered a point that was initially controlled by the spiral wave and after 2.5 s started being influenced by the external stimulation. The plot shows a period of 53.6 ms, which is equal to the stimulation period. This precludes the possibility of the Wenckebach/Mobitz pattern.
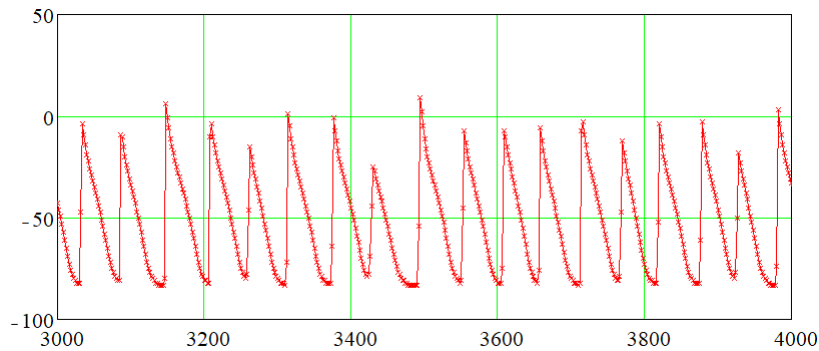

Fig. 6. Transmembrane potential u at the point $x = 25$ mm, $y = 40$ mm. The stimulation current was applied with $0.88 \cdot T_{\mathrm{sw}}$ period from the long line electrode. Horizontal axis is t, ms; vertical axis is u, mV.

We also measured moments of time when the spiral started to drift, T_1, and when it approached the square boundary, T_2 (Table 5). For both electrode locations, we see that the higher the stimulation period was, the later the spiral wave answered to the external stimulation and came to the boundary. In addition, an increase of the period led to a growth in the drift duration (which equals $T_2 - T_1$)

in most of the cases. The only exception was the case $T_{\text{stim}} = 0.985 \cdot T_{\text{sw}}$ with the point electrode, where the spontaneous drift lasted for a very short time and the spiral was far from the boundaries when its induced drift began. The long line electrode demonstrated better results in comparison with the point electrode – the spiral wave began its drift earlier and approached the boundary faster.

The x- and y-components of spiral wave drift velocity were calculated for the case of one line electrode. Total velocity included the spontaneous drift while net velocity did not. We also computed net relative velocity components by dividing the absolute net values by the 1D wave speed V_1: $V_x^{rel} = V_x/V_1$, $V_y^{rel} = V_y/V_1$. This enabled us to assess dimensionless drift velocity. The results are displayed in Table 6. Both velocities V_x and V_y decreased with an increase of stimulation period. Moreover, spiral waves drifted faster in the y-direction than in the x-direction. An increase in the stimulation period caused a change of the V_x sign from positive to negative and, therefore, a turn of the drift direction toward the electrode.

4   Related Work

Simulations of spiral wave dynamics require integration of the differential equations in time, which can be done using explicit or implicit numerical methods. Explicit methods require very small timesteps, each of which is a computationally easy task, and implicit methods are costly in one step. The drift of spiral waves in 2D and 3D media can be a slow process, so it should be studied during about one minute of model time or more. In any case, the total computational cost of one program run is usually big enough to force researchers to utilise parallel computers, libraries and software. The problem of parallel computation of spiral wave dynamics and cardiac electrophysiology has been addressed in several works (see, for example, [14, 19, 15]). Vectorisation can provide an x18 increase in the computation speed, and CPU-based parallelisation can afford an x7 increase [15]. Results on 3D heart modelling obtained by our group previously show that a GPU provided essential acceleration. One model minute of simulations required one day if a GPU-based system was used [16] (TP06 model) and about nine days if a CPU-based system was used [17] (EO model [13] without mechanics; its computational cost is comparable to that of the TP06 model).

5   Discussion and Conclusions

Previously published results on the induced drift of spiral waves in isotropic myocardial models [18] showed the following results. Effective drift occurred for relative stimulation periods between 0.8 and 0.97 if one point electrode or one line electrode is used. The time when the induced drift begins and ends increases with an increase in the period. The drift velocity component orthogonal to the line electrode decreases linearly with an increase in the period. Our results from the present study show a slightly narrower segment of the effective periods (0.88–1.01) and the same dependence between the period and the velocity component.

The case of an anisotropic tissue model where fibres are straight and parallel was also studied [3] for a simple phenomenological model AP [1] of the cardiac muscle. Results of those simulations are close to the results with the isotropic medium and those of the present work. It was shown that the segment of effective periods was the same; however, new spiral waves emerged in many cases depending on the fibre direction and electrode configuration. Mathematically, introducing anisotropy with parallel fibre directions, if wave speed is less across fibres, is similar to a compression of the isotropic medium in the direction orthogonal to the fibres. Therefore, studying heart-specific anisotropy requires research on media with curved fibres.

The present work investigates circular-shaped fibres. This pattern is similar to that observed in the atria of the heart around the pulmonary vein region. There are several such regions in the atria: four pulmonary veins (in the left atrium) and two vena-cava regions (in the right atrium). Therefore, the atrial wall has many regions that are topologically equivalent to obstacles (holes) in the tissue. They can anchor spiral waves and result in arrhythmias, such as atrial tachycardia and flutter. We think that the LVCD methodology, which we study in this paper, could be a potential treatment approach for the re-entry arrhythmias.

A theoretical investigation of the overdrive pacing was done in [10]. A formula linking the relative stimulation period $p = T_{\text{stim}}/T_{\text{sw}}$ and the relative drift velocity component $V_x^{rel} = V_x/V_1$ was proposed for the case of a sole line electrode in isotropic medium: $V_x^{rel} = 1 - p$. Here, the electrode is located at the left border $x = 0$ of the squared medium. We computed the velocity component and compared our results with the theory. We see that theoretical V_x^{rel} decreases from 0.12 ($p = 0.88$) to 0.015 ($p = 0.985$), but simulated V_x^{rel} is about 10–20 times less. This shows that the curved fibre-based anisotropy plays an important role in the overdrive pacing. Generalising the theory of overdrive pacing in anisotropic media would be an interesting topic for future research.

Another theory of overdrive pacing was proposed in [6] for waves with a circular core and for an isotropic medium. Unfortunately, it is not applicable in our case because the wave tip followed a complex trajectory even in isotropy, and our medium is essentially anisotropic.

Recently, we performed studies on spiral wave drift in an isotropic square (non-published). Those simulations used the same Luo–Rudy I model and one long line electrode. The results show that limits of the effective relative stimulation period are 0.87–0.97. We see that our limit of 0.88–1.01 is comparable with that segment, which means that anisotropy with curved fibres almost does not affect the effectiveness of the low-voltage cardioversion.

Limitations of this research are connected with the fact that we did not consider thickness, heterogeneity and curvature of the heart wall. Also, we neglect mechano-electrical feedback, which can play a significant role in spiral wave drift and therefore in overdrive pacing. Our future work will be devoted to overcoming these limitations and to using a more detailed ionic myocardial model, such as TP06, which describes more ionic currents.

Our mesh was large, and the main calculation task involved computation of the right-hand parts of the reaction-diffusion system. An increase of task complexity amplifies the amount of calculations per computing node. We believe that the use of MPI technology will speed up our simulations significantly.

References

1. R.R. Aliev and A.V. Panfilov. A simple two-variable model of cardiac excitation. *Chaos, Solitons and Fractals*, 7(3):293–301, 1996.
2. Bryan J. Caldwell, Mark L. Trew, and Arkady M. Pertsov. Cardiac response to low-energy field pacing challenges the standard theory of defibrillation. *Circulation: Arrhythmia and Electrophysiology*, 8(3):685–693, 2004.
3. Timofei Epanchintsev, Sergei Pravdin, Andrey Sozykin, and Alexander Panfilov. Simulation of overdrive pacing in 2D phenomenological models of anisotropic myocardium. In *Proceedings of the 6th International Young Scientists Conference in HPC and Simulation YSC 2017*, volume 119 of *Procedia Computer Science*, pages 245–254, Kotka, Finland, 2017. Elsevier B.V.
4. E.A. Ermakova, V.I. Krinsky, A.V. Panfilov, and A.M. Pertsov. Interaction between spiral and flat periodic autowaves in an active medium. *Biofizika*, 31(2):318–323, 1986. In Russian.
5. Flavio Fenton and Alain Karma. Vortex dynamics in three-dimensional continuous myocardium with fiber rotation: Filament instability and fibrillation. *Chaos: An Interdisciplinary Journal of Nonlinear Science*, 8(1):20–47, 1998.
6. Georg Gottwald, Alain Pumir, and Valentin Krinsky. Spiral wave drift induced by stimulating wave trains. *Chaos: An Interdisciplinary Journal of Nonlinear Science*, 11(3):487–494, 2001.
7. D. Hornung, V. N. Biktashev, N. F. Otani, T. K. Shajahan, T. Baig, S. Berg, S. Han, V. I. Krinsky, and S. Luther. Mechanisms of vortices termination in the cardiac muscle. *Royal Society Open Science*, 4(3), 2017.
8. J.P. Keener and A.V. Panfilov. A biophysical model for defibrillation of cardiac tissue. *Biophys J.*, 71(3):1335–45, 1996.
9. On-Uma Kheowan, Chi-Keung Chan, Vladimir S. Zykov, Orapin Rangsiman, and Stefan C. Müller. Spiral wave dynamics under feedback derived from a confined circular domain. *Phys. Rev. E*, 64:035201, Aug 2001.
10. V.I. Krinsky and K.I. Agladze. Interaction of rotating waves in an active chemical medium. *Physica D: Nonlinear Phenomena*, 8(1):50 – 56, 1983.
11. Wenwen Li, Crystal M. Ripplinger, Qing Lou, and Igor R. Efimov. Multiple monophasic shocks improve electrotherapy of ventricular tachycardia in a rabbit model of chronic infarction. *Heart Rhythm*, 6(7):1020 – 1027, 2009.
12. C.H. Luo and Y. Rudy. A model of the ventricular cardiac action potential. Depolarization, repolarization, and their interaction. *Circulation Research*, 68(6):1501–1526, 1991.
13. V.S. Markhasin, O. Solovyova, L.B. Katsnelson, Yu. Protsenko, P. Kohl, and D. Noble. Mechano-electric interactions in heterogeneous myocardium: development of fundamental experimental and theoretical models. *Progress in Biophysics and Molecular Biology*, 82(1):207 – 220, 2003.
14. A. Mena, J.M. Ferrero, and J.F. Rodriguez. Computer simulation of the electric activity of the heart using GPU. A multi-scale approach. In *Proceedings of the 41st International Congress on Electrophysiology ICE 2014*, Bratislava, Slovakia, 2014.

15. Kazuo Nakazawa, Tohru Suzuki, Takashi Ashihara, Masashi Inagaki, Tsunetoyo Namba, Takanori Ikeda, and Ryoji Suzuki. *Computational Analysis and Visualization of Spiral Wave Reentry in a Virtual Heart Model*, pages 217–241. Springer Japan, Tokyo, 2000.
16. S. F. Pravdin, H. Dierckx, and A. V. Panfilov. Effect of the form and anisotropy of the left ventricle on the drift of spiral waves. *Biophysics*, 62(2):309–311, Mar 2017.
17. Sergei Pravdin, Konstantin Ushenin, Andrey Sozykin, and Olga Solovyova. Human heart simulation software for parallel computing systems. *Procedia Computer Science*, 66(Supplement C):402 – 411, 2015. 4th International Young Scientist Conference on Computational Science.
18. Sergei F. Pravdin, Timur V. Nezlobinsky, and Alexander V. Panfilov. Modelling of low-voltage cardioversion using 2D isotropic models of the cardiac tissue. In *Proceedings of the International Conference Days on Diffraction 2017*, pages 276–281, Saint-Petersburg, Russia, 2017.
19. Daisuke Sato, Yuanfang Xie, James N. Weiss, Zhilin Qu, Alan Garfinkel, and Allen R. Sanderson. Acceleration of cardiac tissue simulation with graphic processing units. *Medical & Biological Engineering & Computing*, 47(9):1011–1015, Sep 2009.
20. S. Sinha and S. Sridhar. *Patterns in Excitable Media: Genesis, Dynamics, and Control*. Taylor & Francis, 2014.
21. Michael O. Sweeney. Antitachycardia pacing for ventricular tachycardia using implantable cardioverter defibrillators. *Pacing and Clinical Electrophysiology*, 27(9):1292–1305, 2004.
22. K. H. W. J. Ten Tusscher and A. V. Panfilov. Reentry in heterogeneous cardiac tissue described by the Luo–Rudy ventricular action potential model. *American Journal of Physiology - Heart and Circulatory Physiology*, 284(2):H542–H548, 2003.
23. Kirsten HWJ Ten Tusscher and Alexander V Panfilov. Alternans and spiral breakup in a human ventricular tissue model. *American Journal of Physiology-Heart and Circulatory Physiology*, 291(3):1088–1100, 2006.
24. Mark S. Wathen et al. Prospective randomized multicenter trial of empirical antitachycardia pacing versus shocks for spontaneous rapid ventricular tachycardia in patients with implantable cardioverter-defibrillators. *Circulation*, 110(17):2591–2596, 2004.
25. Seth H. Weinberg, Kelly C. Chang, Renjun Zhu, Harikrishna Tandri, Ronald D. Berger, Natalia A. Trayanova, and Leslie Tung. Defibrillation success with high frequency electric fields is related to degree and location of conduction block. *Heart Rhythm*, 10(5):740 – 748, 2013.
26. K.F. Wenckebach. *De Analyse van den onregelmatigen Pols. III. Over eenige Vormen van Allorythmie en Bradykardie*, volume 2 of *Nederlandsch Tijdschrift voor Geneeskunde*. Amsterdam, 1898. (In Dutch).
27. Hong Zhang, Bambi Hu, and Gang Hu. Suppression of spiral waves and spatiotemporal chaos by generating target waves in excitable media. *Phys. Rev. E*, 68:026134, Aug 2003.
28. V.S. Zykov, A.S. Mikhailov, and S.C. Müller. Controlling spiral waves in confined geometries by global feedback. *Phys. Rev. Lett.*, 78:3398–3401, Apr 1997.